Mechanism and Machine Theory 104 (2016) 222–233

Contents lists available at ScienceDirect

Mechanism and Machine Theory

journal homepage: www.elsevier.com/locate/mechmt

Kinematics analysis of a novel over-constrained three degree-of-freedom spatial parallel manipulator

Bin Li [a,b], Yangmin Li [a,b,*], Xinhua Zhao [b]

[a] Department of Electromechanical Engineering, Faculty of Science and Technology, University of Macau, Avenida da Universidade, Taipa, Macau
[b] Tianjin Key Laboratory for Advanced Mechatronic System Design and Intelligent Control, School of Mechanical Engineering, Tianjin University of Technology, Tianjin 300384, China

ARTICLE INFO

Article history:
Received 7 March 2014
Received in revised form 5 May 2016
Accepted 3 June 2016
Available online 10 June 2016

Keywords:
Spatial parallel manipulators
Kinematic analysis
Workspace analysis

ABSTRACT

In this paper, a novel over-constrained three degree-of-freedom (DOF) spatial parallel manipulator (SPM) is proposed. The architecture of the SPM is comprised of a moving platform attached to a base through two revolute-prismatic-universal jointed serial linkages and one spherical-prismatic-revolute jointed serial linkage. The prismatic joints are considered to be actively actuated. Kinematics and performance of the SPM are studied systematically. Firstly, the structure characteristics and DOF of this SPM are analyzed based on screw theory. Secondly, both of the inverse and forward displacements are derived by analytic formulae. Then, the Jacobian matrix of the mechanism is derived. Thirdly, the workspace of the mechanism is obtained based on the forward position analysis. Finally, the performance analysis of the mechanism is analyzed by pressure angles between limbs and some conclusions are given.

1. Introduction

In recent years, lower-mobility SPMs have been extensively studied. Compared with 6-DOF parallel manipulators, lower-mobility mechanisms possess such merits as simpler mechanical design, lower manufacturing cost, and larger workspace, in addition to the inherent advantages of the general parallel manipulators in terms of high accuracy, high stiffness, high velocity, high dynamic performance, big load to weight ratio, low moving inertia and little accumulation of positional errors. A lower-mobility SPM with 3-DOF is the focus of the current trend in the research community, and various forms of 3-DOF SPM have been presented.

Hunt [1] presented a 3-RPS parallel manipulator, which has two rotational and one translational DOF, up to now this mechanism has been widely studied and used in practice. Clavel [2] proposed the well-known 3-DOF translational SPM Delta robot, one of the most commercially successful parallel manipulators, which is commonly used in pick-and-place applications. Liu [3] developed a type of new 3-DOF SPM with three nonidentical chains, the moving platform has two translational and a rotational freedoms, both the inverse and forward kinematics problems and singularity are described. Zhang [4] studied a novel 3-DOF SPM used for machining applications, the structure of the mechanism is comprised of three active limbs and one passive limb aiming to achieve a greater stiffness and more effective 3-DOF motions. Xie [5] proposed a decoupled 3-DOF parallel tool head without parasitic motions, and the kinematic optimization of the tool head was carried out. Rodriguez-Leal and Dai [6,7] proposed a 3-CUP SPM,and studied the mobility of the mechanism. Recently, the kinematic problems including position analysis, singularity analysis

* Corresponding author at: Department of Electromechanical Engineering, Faculty of Science and Technology, University of Macau, Avenida da Universidade, Taipa, Macau.
E-mail address: YMLi@umac.mo (Y. Li).

http://dx.doi.org/10.1016/j.mechmachtheory.2016.06.003
0094-114X/

and workspace analysis of the 3-CUP SPM have been investigated by Cuan-Urquizo [8]. Recently, Zhang [9] designed a novel 3-DOF parallel robotic manipulator with decoupled motions, and examined the kinematic modeling of the parallel manipulator in terms of inverse and forward kinematics study, velocity analysis, singularity analysis, as well as stiffness analysis. Besides these new 3-DOF SPMs mentioned above, some other 3-DOF architectures can be found in the literature [10–18].

In this paper, a novel over-constrained 3-DOF SPM 2-RPU&SPR with one degree of translational freedom and two degrees of rotational freedom is proposed. The paper is arranged in the following structure. Firstly, the structure characteristics and DOF of this SPM are analyzed based on screw theory in Section 2 and Section 3. Then, both of the inverse and forward displacements are derived by analytic formulae, and some numerical examples are depicted in Section 4. In Section 5, the Jacobian matrix of the mechanism is obtained. Thirdly, the workspace of the mechanism is obtained based on the forward position analysis [20], and several 3D shapes of the reachable workspace of the mechanism is obtained using computer code programming in Section 6. Furthermore, the performance analysis of the mechanism is analyzed by using definition of pressure angles between limbs in Section 7. Finally, Section 8 presents some conclusions and future research on this 2-RPU&SPR SPM, and the possible practical application of the mechanism according to the analysis of the platform motion performances.

2. An over-constrained 2-RPU&SPR SPM and its structure characteristics

As shown in Fig. 1, the proposed over-constrained 3-DOF SPM 2-RPU & SPR consists of a base platform and a moving platform connected by two identical RPU limbs and one SPR limb. Here, R, U and S represent the revolute, universal and spherical joints, and the underlined P denotes the actuated prismatic joint. Place the reference frame *B-xyz* attached to the base and the moving frame *A-uvw* attached to the moving platform with *B* and *A* being the origins located at the midpoint of lines B_1B_2 and A_1A_3 with the *x* and *u* axes being parallel to B_1B_2 and A_1A_3, and the *z* and *w* axes being normal to the base platform and the moving platform. Here, B_i $(i = 1,2)$ and A_3 are the intersection of the axes of the revolute joints and actuated prismatic joints, B_3 is the center of the spherical joint, A_1 and A_2 are the centers of the universal joints, respectively.

For the proposed mechanism, the two identical RPU limbs are in the same plane *of Bxy* and axes of the two revolute joints are parallel to *y* axis as shown in Fig. 2. It should be pointed out that, two universal joints of RPU limbs are shared and connected on the moving platform. The axis of revolute joint of the SPR limb is parallel to *u* axis. Due to these joints arrangement mentioned above, the moving platform of the presented 3-DOF SPM exhibits a motion such that one of its points tracks a planar curve (2DOF) and orientation of the platform is controlled about an axis tangent to that curve (1DOF). Up to now, there is no such type parallel mechanism with these motion outputs in literature.

The orientation matrix of the *A-uvw* with respect to the *B-xyz* can be formulated by three Euler angles ψ,ϕ and θ satisfying *x-z-y* conventions:

$$\mathbf{R} = \begin{bmatrix} c\theta c\phi & s\psi s\theta - c\psi c\theta s\phi & c\psi s\theta + s\psi c\theta s\phi \\ s\phi & c\psi c\phi & -s\psi c\phi \\ -s\theta c\phi & s\psi c\theta + c\psi s\theta s\phi & c\psi c\theta - s\psi s\theta s\phi \end{bmatrix} = \begin{bmatrix} u_x & v_x & w_x \\ u_y & v_y & w_y \\ u_z & v_z & w_z \end{bmatrix} = [\mathbf{u}\ \mathbf{v}\ \mathbf{w}] \tag{1}$$

where $\boldsymbol{u}$, $\boldsymbol{v}$ and $\boldsymbol{w}$ are the unit vectors of the frame *A-uvw* with respect to the frame *B-xyz*, "*s*" and "*c*" here denote sin and cos functions.

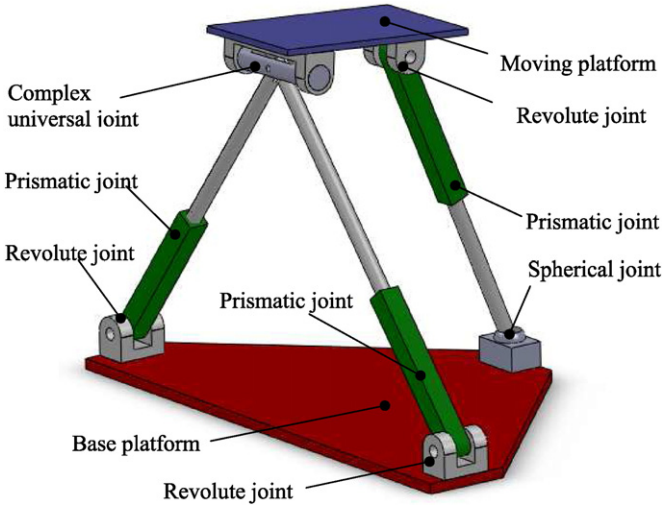

Fig. 1. CAD model of the proposed 3-DOF SPM 2-RPU&SPR.

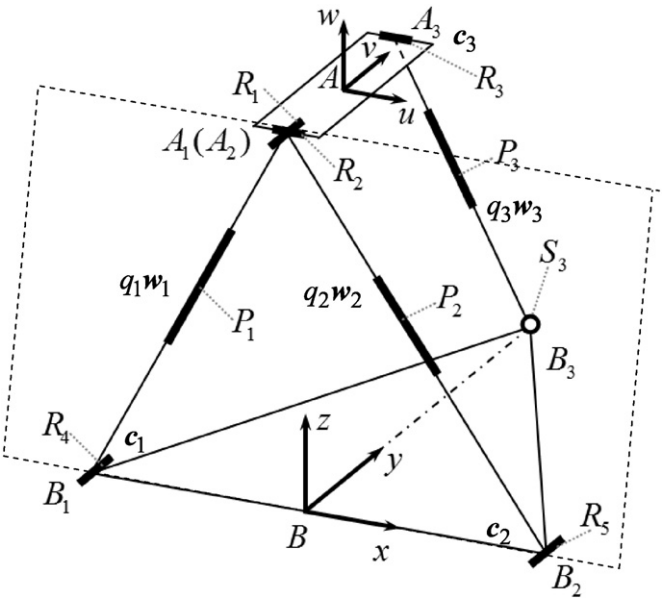

Fig. 2. Schematic model of the mechanism.

3. Mobility analysis via screw theory

The mobility of the 2-RPU&SPR SPM is determined by the combined effect of the three limb constraint forces/couples. In this paper, reciprocal screw theory is used to analyze constraint forces exerted on the moving platform. In a parallel manipulator, the reciprocal screws associated with a serial limb represent the wrench constraints imposed on the moving platform by the serial limb. For a complete description of computing the mobility of SPMs using this method the reader can refer to Ref. [11,12].

The kinematic screw is often denoted in the form of Plücker homogeneous coordinates:

$$\mathbf{\$} = (L \quad M \quad N \quad P \quad Q \quad R) \tag{2}$$

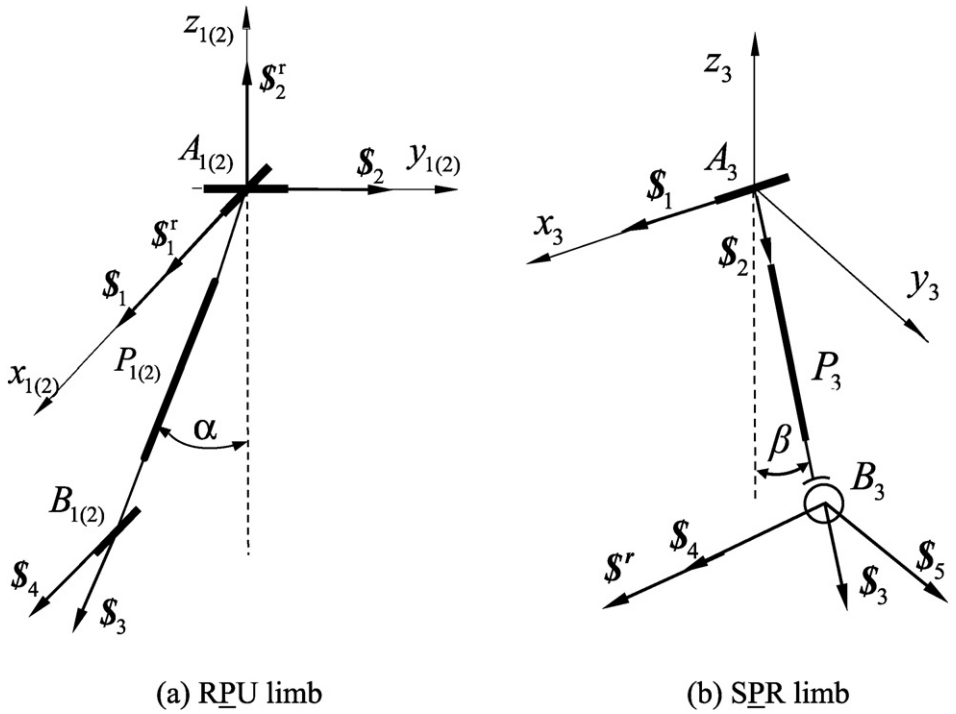

Fig. 3. Twist systems of RPU limb and SPR limb.

where the first three components denote the angular velocity, the last three components denote the linear velocity of a point in the rigid body that is instantaneously coincident with the origin of the coordinate system. Similarly, $\mathbf{\$}^r$ is defined as

$$\mathbf{\$}^r = (L^r \quad M^r \quad N^r \quad P^r \quad Q^r \quad R^r) \tag{3}$$

where the first three components denote the resultant force and the last three components denote the resultant moment about the origin of the coordinate system.

Two screws, $\mathbf{\$}$ and $\mathbf{\$}^r$, are called to be reciprocal if they satisfy the equation:

$$LP^r + MQ^r + NR^r + PL^r + QM^r + RN^r = 0 \tag{4}$$

(a) RPU limb (b) SPR limb.

Without losing generality, a local coordinate system A_i-$x_iy_iz_i$, $i = 1,2,3$ is established for each limb as shown in Fig. 3. The limb twist system of the RPU limb in Fig. 3(a) is given by

$$\begin{aligned}
\mathbf{\$}_1 &= (1 \quad 0 \quad 0 \quad 0 \quad 0 \quad 0)\\
\mathbf{\$}_2 &= (0 \quad 1 \quad 0 \quad 0 \quad 0 \quad 0)\\
\mathbf{\$}_3 &= (0 \quad 0 \quad 0 \quad 0 \quad -\sin\alpha \quad -\cos\alpha)\\
\mathbf{\$}_4 &= (1 \quad 0 \quad 0 \quad 0 \quad -\boldsymbol{q}_{1(2)}\cos\alpha \quad \boldsymbol{q}_{1(2)}\sin\alpha)
\end{aligned} \tag{5}$$

where $q_i = \|A_iB_i\|$, $i = 1,2,3$.

Using the reciprocity between twist and wrench, the RPU limb constraint system can be calculated by

$$\begin{aligned}
\mathbf{\$}_1^r &= (1 \quad 0 \quad 0 \quad 0 \quad 0 \quad 0)\\
\mathbf{\$}_2^r &= (0 \quad 0 \quad 0 \quad 0 \quad 0 \quad 1)
\end{aligned} \tag{6}$$

With $\mathbf{\$}_1^r$ denoting a constraint force passing through the universal joint center and being parallel to the axis of joint screw $\mathbf{\$}_1$, and $\mathbf{\$}_2^r$ denoting a constraint couple whose direction is perpendicular to the axes of joint screws $\mathbf{\$}_1$ and $\mathbf{\$}_2$.

The limb twist system of the SPR limb in Fig. 3(b) is given by

$$\begin{aligned}
\mathbf{\$}_1 &= (1 \quad 0 \quad 0 \quad 0 \quad 0 \quad 0)\\
\mathbf{\$}_2 &= (0 \quad 0 \quad 0 \quad 0 \quad \sin\boldsymbol{\beta} \quad -\cos\boldsymbol{\beta})\\
\mathbf{\$}_3 &= (0 \quad \sin\boldsymbol{\beta} \quad -\cos\boldsymbol{\beta} \quad 0 \quad 0 \quad 0)\\
\mathbf{\$}_4 &= (1 \quad 0 \quad 0 \quad 0 \quad -q_3\cos\boldsymbol{\beta} \quad -q_3\sin\boldsymbol{\beta})\\
\mathbf{\$}_5 &= (0 \quad -\cos\boldsymbol{\beta} \quad -\sin\boldsymbol{\beta} \quad -q_3 \quad 0 \quad 0)
\end{aligned} \tag{7}$$

The SPR limb constraint system is

$$\mathbf{\$}^r = (1 \quad 0 \quad 0 \quad 0 \quad -\boldsymbol{q}_3\cos\boldsymbol{\beta} \quad -\boldsymbol{q}_3\sin\boldsymbol{\beta}) \tag{8}$$

The system in Eq. (8) presents a constraint force passing through the spherical joint center and being parallel to the axis of joint screw $\mathbf{\$}_1$ in every configuration.

From Eqs. (6) and (8), we can see that two RPU limbs restrict a translational DOF of the moving platform along the direction of the constraint force and a rotational DOF around the axis of the constraint couple. The SPR limb restricts a translational DOF of the moving platform along the direction of the constraint force. So, the 2-RPU&SPR SPM owns one degree of translational freedom and two degrees of rotational freedom.

4. Inverse and forward position analyses

4.1. Inverse position analysis

Inverse position analysis of the 2-RPU & SPR SPM involves the determination of the limb lengths given the pose of the moving platform.

In the *B-xyz*, the position vector $\boldsymbol{r} = (x{\cdot}y{\cdot}z)^{\mathrm{T}}$ of A can be expressed by the loop closure equation

$$\boldsymbol{r} = \mathbf{b}_i + q_i\mathbf{w}_i - \mathbf{a}_i \qquad i = 1,2,3 \tag{9}$$

where $\mathbf{a}_i = \mathbf{R}\mathbf{a}_{i0}$ are the position vectors of A_i measured in *A-uvw*, $\mathbf{a}_{10} = \mathbf{a}_{20} = a_1(0 \quad -1 \quad 0)^{\mathrm{T}}$, $\mathbf{a}_{30} = a_2(0 \quad 1 \quad 0)^{\mathrm{T}}$,$a_i$ is the distance of $\|AA_i\|$, here, $a_1 = a_2 = a_3 = a$, and $\mathbf{b}_1 = b_1(-1 \quad 0 \quad 0)^{\mathrm{T}}$, $\mathbf{b}_2 = b_2(1 \quad 0 \quad 0)^{\mathrm{T}}$,$\mathbf{b}_3 = b_3(0 \quad 1 \quad 0)^{\mathrm{T}}$are the position vectors of B_i measured in *B-xyz* with b_i being the distance of $\|BB_i\|$, here, $b_1 = b_2 = b$. q_i and $\boldsymbol{w}_i$ are the length and unit vector of limb i.

Note that for the RPU limb, the constraint imposed by the revolute joint restricts both $\boldsymbol{w}_i$ and $\boldsymbol{b}_i$ to be normal to the unit vector $\boldsymbol{c}_i$ of the revolute joint axis. Thus, taking the dot product with $\boldsymbol{c}_i$ on both sides of Eq. (9), leads to

$$(\mathbf{r}+\mathbf{a}_i)^T\mathbf{c}_i = 0 \quad i = 1,2 \tag{10}$$

where $\mathbf{c}_1 = \mathbf{c}_2 = (0 \quad 1 \quad 0)^{\mathrm{T}}$.

Similarly, for the SPR limb, the constraint imposed by the revolute joint restricts both $\boldsymbol{w}_3$ and $\boldsymbol{a}_3$ to be normal to the unit vector $\boldsymbol{c}_3$ of the revolute joint axis. Thus, taking the dot product with $\boldsymbol{c}_i$ on both sides of Eq. (9), leads to

$$(\mathbf{r}-\mathbf{b}_i)^T\mathbf{c}_i = 0 \quad i = 3 \tag{11}$$

where $\mathbf{c}_3 = \mathbf{R}\mathbf{c}_{30}, \mathbf{c}_{30} = (1 \quad 0 \quad 0)^{\mathrm{T}}$.

According to the geometric constraint of the mechanism, axis of the universal joint R_2 can just only move in the plane *Bxz* as shown in Fig. 2, so another equation can be formulated

$$u_y = 0 \tag{12}$$

Based on Eqs. (10), (11), and (12), we can obtain

$$\phi = 0 \tag{13}$$

$$y = a\cos(\psi) \tag{14}$$

$$x = z\tan(\theta) \tag{15}$$

Here ϕ,*y*, and *x* represent the parasitic motions of the moving platform. The parasitic motions lead to complex kinematics, require real-time compensation, increase difficulty in calibration, and even result in damage to the SPM. For a given set of unconstrained variables$(\psi \quad \theta \quad z)$, the parasitic motion of the mechanism can be calculated through Eqs. (13), (14), and (15). Then, the limb length can be calculated as

$$q_i = |\mathbf{r}-\mathbf{b}_i+\mathbf{a}_i|, \quad i = 1,2,3 \tag{16}$$

4.2. Forward position analysis

The forward position analysis of the mechanism is concerned with the determination of the moving platform pose given the limb lengths. Firstly, taking Euclidean norm on both sides of Eq. (16), and implementing necessary addition and subtraction, yields

$$q_1^2 = [z\tan(\theta)-a\sin(\psi)\sin(\theta)+b]^2 + [z-a\sin(\psi)\cos(\theta)]^2 \tag{17}$$

$$q_2^2 = [z\tan(\theta)-a\sin(\psi)\sin(\theta)-b]^2 + [z-a\sin(\psi)\cos(\theta)]^2 \tag{18}$$

$$q_3^2 = [z\tan(\theta)+a\sin(\psi)\sin(\theta)]^2 + [2a\cos(\psi)-b_3]^2 + [z+a\sin(\psi)\cos(\theta)]^2 \tag{19}$$

1) If $q_1 \neq q_2$, implementing subtraction and addition for Eq. (17) and Eq. (18), yields

$$z = f_1 c\tan(\theta) + a\sin(\psi)\cos(\theta) \tag{20}$$

$$q_1^2 + q_2^2 = \frac{2z^2}{\cos(\theta)^2} - \frac{4az\sin(\psi)}{\cos(\theta)} + 2a^2\sin(\psi)^2 + 2b^2 \tag{21}$$

where $f_1 = \frac{q_1^2-q_2^2}{4b}$.

Then, substituting Eq. (20) into Eqs. (21) and (19) gives

$$\sin(\theta) = \pm\sqrt{\frac{2f_1^2}{q_1^2+q_2^2-2b^2}} \tag{22}$$

$$q_3^2 = \frac{f_1^2}{\sin(\theta)^2} + 4af_1\frac{\sin(\psi)}{\sin(\theta)} - 4ab_3\cos(\psi) + 4a^2 + b_3^2 \tag{23}$$

2) If $q_1 = q_2$, implementing subtraction for Eq. (17) and Eq. (18), yields

$$\theta = 0 \tag{24}$$

Eqs. (17), (19) can be rewritten as

$$z = \sqrt{q_1^2 - b^2} + a\sin(\psi) \tag{25}$$

$$q_3^2 = [2a\cos(\psi) - b_3]^2 + [z + a\sin(\psi)]^2 \tag{26}$$

Then, substituting Eq. (25) into Eq. (26) gives

$$q_3^2 = 4a^2 + b_3^2 + f_2^2 + 4af_2\sin(\psi) - 4ab_3\cos(\psi) \tag{27}$$

where $f_2 = \sqrt{q_1^2 - b^2}$.

Lastly, given a set of limb lengths($q_1 \quad q_2 \quad q_3$), if $q_1 \neq q_2$,we can solve for θ and ψ by using Eqs. (22) and (23). Thus, the orientation matrix **R** can be generated, leading to the solution of x, y and z by using Eqs. (15), (14) and (20). If $q_1 = q_2$, we can solve for θ and ψ by using Eqs. (24) and (25). The orientation matrix **R** can be generated, leading to the solution of x, y and z by using Eqs. (15), (14) and (25).

From Section 4.1 and Section 4.2, we can see that for the proposed 2-RPU&SPR SPM in this paper, both the inverse and the forward position analyses of the mechanism can be calculated directly though analytical method, and the parasitic motions of the moving platform can be expressed in explicit way, which is extremely significant for the possible practical application of this kind of mechanism.

4.3. Numerical examples

The architectural parameters of a 2-RPU&SPR SPM are selected as: $a = 100\ mm$, $b = 300\ mm$, $b3 = 500\ mm$. For the inverse position analysis, given four different sets of inputs($\psi \quad \theta \quad z$), output parameters can be calculated as shown in Table 1, and Fig. 4 depicts the configurations associated with these solutions. For the forward position analysis, in order to prove the correctness of the algorithms for the inverse and forward position analyses, two solutions for the inverse position analysis are deliberately used as the inputs ($q_1 \quad q_2 \quad q_3$) to the forward position analysis, output parameters can be calculated as shown in Table 2, and Fig. 5 depicts the configurations associated with these solutions.

The results of the forward position analysis shown in Fig. 5 (a) and (c) are consistent with the results of the inverse position analysis shown in Fig. 4 (a) and (d) respectively, two numerical examples are provided to demonstrate the correctness of the algorithm. Note that in Fig. 5 (b) and (d) the values of z are negative, the corresponding configurations merely make sense in mathematics, therefore they should be regarded as the extraneous solutions.

5. Jacobian matrix of the mechanism

Differentiating Eq. (9) with respect to time yields

$$\dot{\mathbf{r}} = \dot{q}_i\mathbf{w}_i + \boldsymbol{\omega}_i \times q_i\mathbf{w}_i - \boldsymbol{\omega} \times \mathbf{a}_i \quad i = 1,2,3 \tag{28}$$

where $\dot{q}_i$ is the velocity of the ith linear actuator, and $\boldsymbol{\omega}_i$ represents the three-dimensional angular velocity of link A_iB_i, "×" denotes the cross product between vectors, $\dot{\mathbf{r}} = (\dot{x} \quad \dot{y} \quad \dot{z})^{\mathrm{T}}$and $\boldsymbol{\omega} = (\omega_x \quad \omega_y \quad \omega_z)^{\mathrm{T}}$represents the three-dimensional linear and angular velocity of the moving platform, respectively.

Table 1
Inverse position analysis of the mechanism.

	Intputs			Outputs				
	ψ (deg.)	θ (deg.)	z (mm)	$q1$ (mm)	$q2$ (mm)	$q3$ (mm)	x (mm)	y (mm)
(a)	25	35	700	1014.5651	685.7525	951.7624	490.1453	90.6308
(b)	−25	35	700	1096.7629	765.2621	872.5787	490.1453	90.6308
(c)	25	−35	700	685.7525	1014.5651	951.7624	−490.1453	90.6308
(d)	−25	−35	700	765.2621	1096.7629	872.5787	−490.1453	90.6308

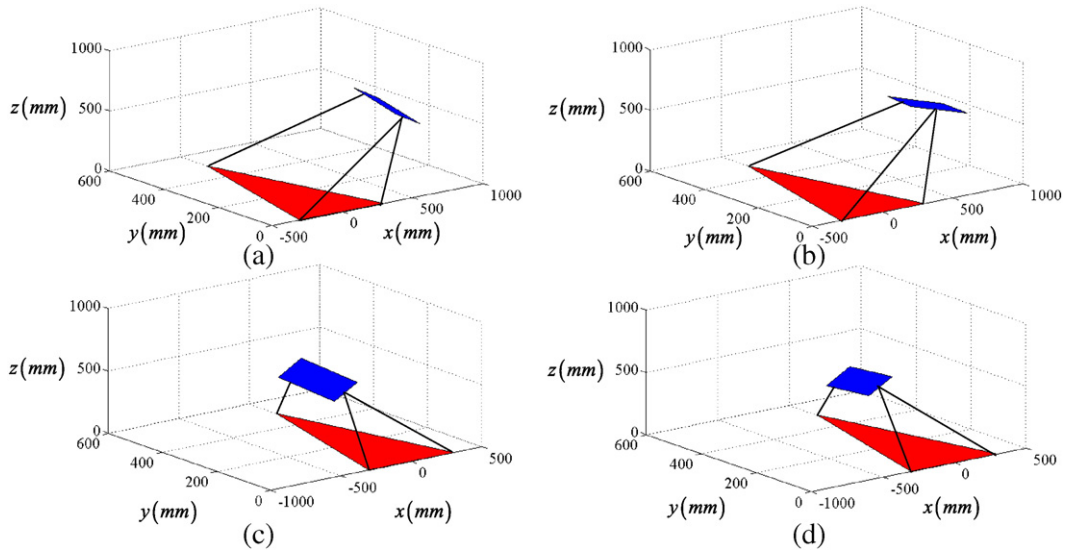

Fig. 4. Different configurations for inverse position.

The passive variable $\boldsymbol{\omega}_i$ can be eliminated by dot multiplying both sides of Eq. (28) with $\mathbf{w}_i$, which gives

$$\dot{q}_i = \mathbf{w}_i\dot{\mathbf{r}} + \boldsymbol{\omega}(\mathbf{a}_i \times \mathbf{w}_i) \quad i = 1,2,3 \tag{29}$$

When the manipulator is away from singularities, Eq. (29) can be written in the matrix form

$$\dot{\mathbf{q}}_a = \mathbf{J}_a\dot{\mathbf{X}} \tag{30}$$

where $\dot{\mathbf{q}}_a = \begin{bmatrix} \dot{q}_1 \\ \dot{q}_2 \\ \dot{q}_3 \end{bmatrix}$, $\dot{\mathbf{X}} = \begin{bmatrix} \dot{\mathbf{r}} \\ \boldsymbol{\omega} \end{bmatrix}$, $\mathbf{J}_a = \begin{bmatrix} \mathbf{w}_1^{\mathrm{T}} & (\mathbf{a}_1 \times \mathbf{w}_1)^{\mathrm{T}} \\ \mathbf{w}_2^{\mathrm{T}} & (\mathbf{a}_2 \times \mathbf{w}_2)^{\mathrm{T}} \\ \mathbf{w}_3^{\mathrm{T}} & (\mathbf{a}_3 \times \mathbf{w}_3)^{\mathrm{T}} \end{bmatrix}$

Eq. (30) represents the inverse velocity solution for the 2-RPU&SPR SPM. It should be noted that the linear and angular velocity components of the moving platform are not all independent since the mechanism possesses only 3-DOF.

Differentiating Eqs. (10) and (11) with respect to time, respectively, yields

$$\mathbf{c}_i \cdot \dot{\mathbf{r}} + (\mathbf{c}_i \times \mathbf{a}_i) \cdot \boldsymbol{\omega} = 0 \quad i = 1,2 \tag{31}$$

$$\mathbf{c}_i \cdot \dot{\mathbf{r}} + [\mathbf{c}_i \times (\mathbf{r} - \mathbf{b}_i)] \cdot \boldsymbol{\omega} = 0 \quad i = 3 \tag{32}$$

When the manipulator is away from singularities, Eqs. (31) and (32) can be written in the matrix form

$$0 = \mathbf{J}_c\dot{\mathbf{X}} \tag{33}$$

where $\mathbf{J}_c = \begin{bmatrix} \mathbf{c}_1^{\mathrm{T}} & (\mathbf{c}_1 \times \mathbf{a}_1)^{\mathrm{T}} \\ \mathbf{c}_2^{\mathrm{T}} & (\mathbf{c}_2 \times \mathbf{a}_2)^{\mathrm{T}} \\ \mathbf{c}_3^{\mathrm{T}} & [\mathbf{c}_3 \times (\mathbf{r} - \mathbf{b}_3)]^{\mathrm{T}} \end{bmatrix}$ and 0 denotes a 3×1 zero matrix.

Table 2
Forward position analysis of the mechanism.

	Intputs			Outputs				
	$q1$ (mm)	$q2$ (mm)	$q3$ (mm)	ψ (deg.)	θ (deg.)	x (mm)	y (mm)	z (mm)
Case (a)	1014.5651	685.7525	951.7624	25	35	490.1453	90.6308	700
				141.7712	−35	430.4117	−78.5546	−614.6917
Case (b)	765.2621	1096.7629	872.5787	−25	−35	−490.1453	90.6308	700
				96.7176	35	−457.4218	−11.6975	−653.2660

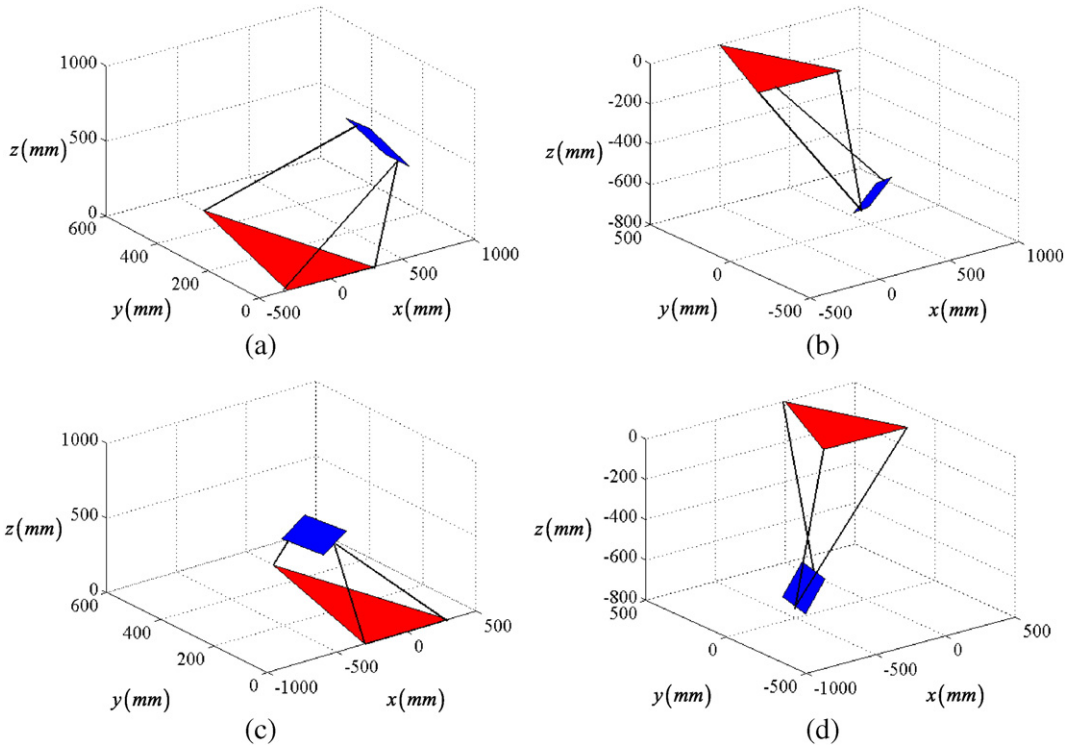

Fig. 5. Different configurations for forward position, Case (*a*): (*a*), (*b*). Case (*b*): (*c*), (*d*).

Eq. (33) represents constraint equations imposed by the topology of the limbs or by passive kinematic chains. Complementing Eq. (30) with Eq. (33) yields

$$\dot{\mathbf{q}} = \mathbf{J}_o \dot{\mathbf{X}} \tag{34}$$

where $\dot{\mathbf{q}} = \begin{bmatrix} \dot{\mathbf{q}}_a \\ 0 \end{bmatrix}$, $\mathbf{J}_o = \begin{bmatrix} \mathbf{J}_a \\ \mathbf{J}_c \end{bmatrix}$ is the overall Jacobian matrix of the mechanism.

Differentiating Eqs. (13), (14) and (15) with respect to time, respectively, yields

$$\dot{\phi} = 0 \tag{35}$$

$$\dot{y} = -a \sin(\psi)\dot{\psi} \tag{36}$$

$$\dot{x} = \dot{z} \tan(\theta) + z \sec^2(\theta)\dot{\theta} \tag{37}$$

Note that differentiating the orientation matrix $\mathbf{R}$ with respect to time yields

$$\dot{\mathbf{R}} = \mathbf{S}(\omega)\mathbf{R} \tag{38}$$

where $\mathbf{S}(\omega) = \begin{bmatrix} 0 & -\omega_z & \omega_y \\ \omega_z & 0 & -\omega_x \\ -\omega_y & \omega_x & 0 \end{bmatrix}$

Then, $\boldsymbol{\omega}$ can be expressed by $\dot{\psi}$and $\dot{\theta}$ through Eq. (38)

$$\boldsymbol{\omega} = \begin{bmatrix} \cos\theta & 0 \\ 0 & 1 \\ -\sin\theta & 0 \end{bmatrix} \begin{bmatrix} \dot{\psi} \\ \dot{\theta} \end{bmatrix} \tag{39}$$

Let $\dot{\mathbf{x}} = (\dot{\psi} \quad \dot{\theta} \quad \dot{z})^{\mathrm{T}}$, the following relation can be calculated by Eqs. (35), (36), (37) and (39)

$$\dot{\mathbf{X}} = \mathbf{J}_r \dot{\mathbf{x}} \tag{40}$$

where $\mathbf{J}_r = \begin{bmatrix} 0 & z\sec^2\theta & \tan\theta \\ -a\sin\psi & 0 & 0 \\ 0 & 0 & 1 \\ \cos\theta & 0 & 0 \\ 0 & 1 & 0 \\ -\sin\theta & 0 & 0 \end{bmatrix}$.

In view of Eqs. (30) and (40), we can get

$$\dot{\mathbf{q}} = \mathbf{J}\dot{\mathbf{x}} \tag{41}$$

where $\mathbf{J} = \mathbf{J}_a\mathbf{J}_r$ is the 3×3 Jacobian matrix which includes the effect of the mechanical constraints on the mechanism, $\boldsymbol{J}$ is called the constrained Jacobian matrix of 2-RPU&SPR SPM.

6. Workspace analysis

In this section, the parasitic motion workspace and the reachable workspace of the 2-RPU&SPR SPM are obtained based on the forward position analysis. From Section 4, we can see that given a set of limb lengths$(q_1 \quad q_2 \quad q_3)$, the other parameters including parasitic motions can be calculated directly by corresponding equations. So when the restrictions to the limb lengths are set up, the parasitic motion workspace and the reachable workspace of the mechanism can be obtained. It should be pointed out that seldom SPMs can obtain the workspace through forward position analysis, this is also one novel contribution in this work.

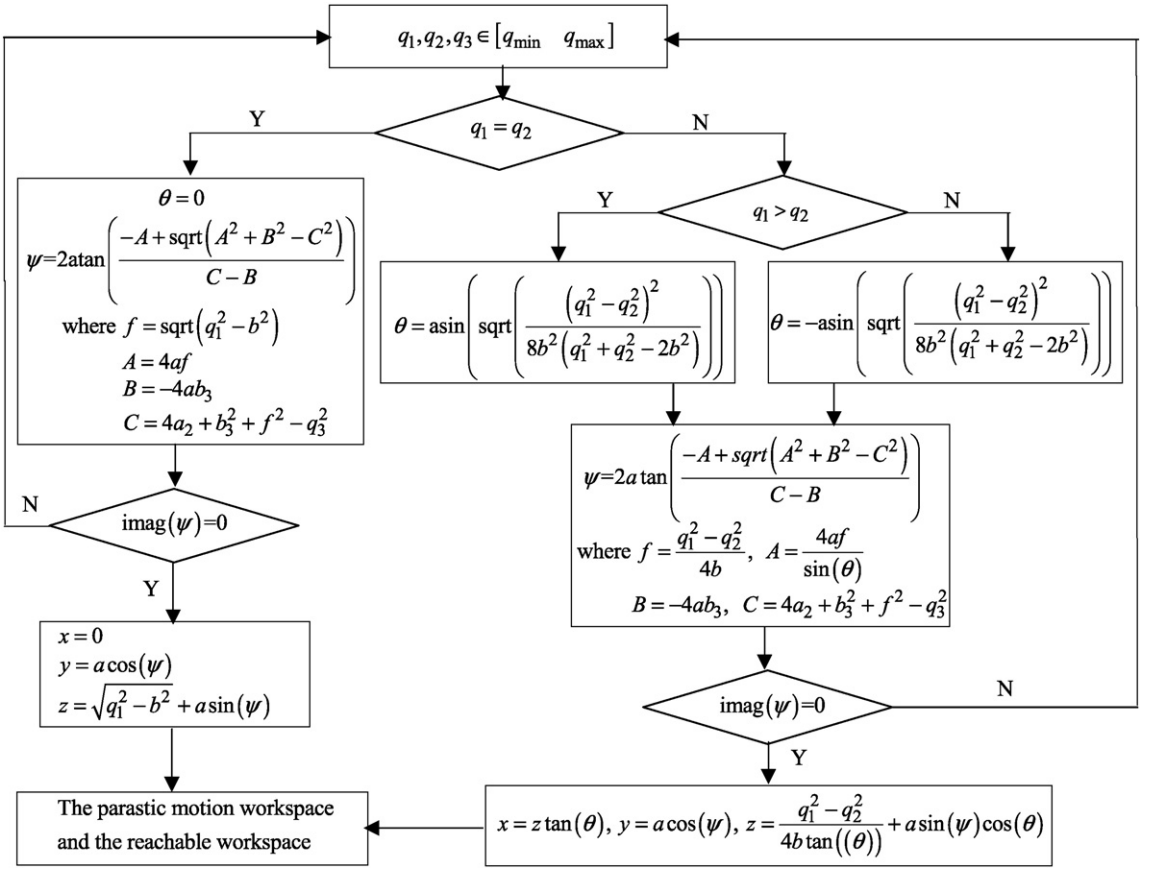

Fig. 6. Flow chart of the reachable workspace calculation.

6.1. Algorithms

The reachable workspace calculating process is shown in Fig. 6.

6.2. Case studies

The architectural parameters of a 2-RPU&SPR parallel manipulator are selected as: $a = 100$ mm, $b = 300$ mm, $b_3 = 500$ mm, 600 mm ≤ q_1 ≤ 900 mm, 600 mm ≤ q_2 ≤ 900 mm, 600 mm ≤ q_3 ≤ 900 mm. The workspace of the manipulator can be generated by a MATLAB program. The parasitic motion workspace of the mechanism as shown in Fig.7(c) and Fig. 7(d). The reachable workspace of the mechanism as shown in Fig. 7(a), Fig. 7(b), Fig. 7(e). And the Fig. 7(f) shows the positional workspace of the moving platform.

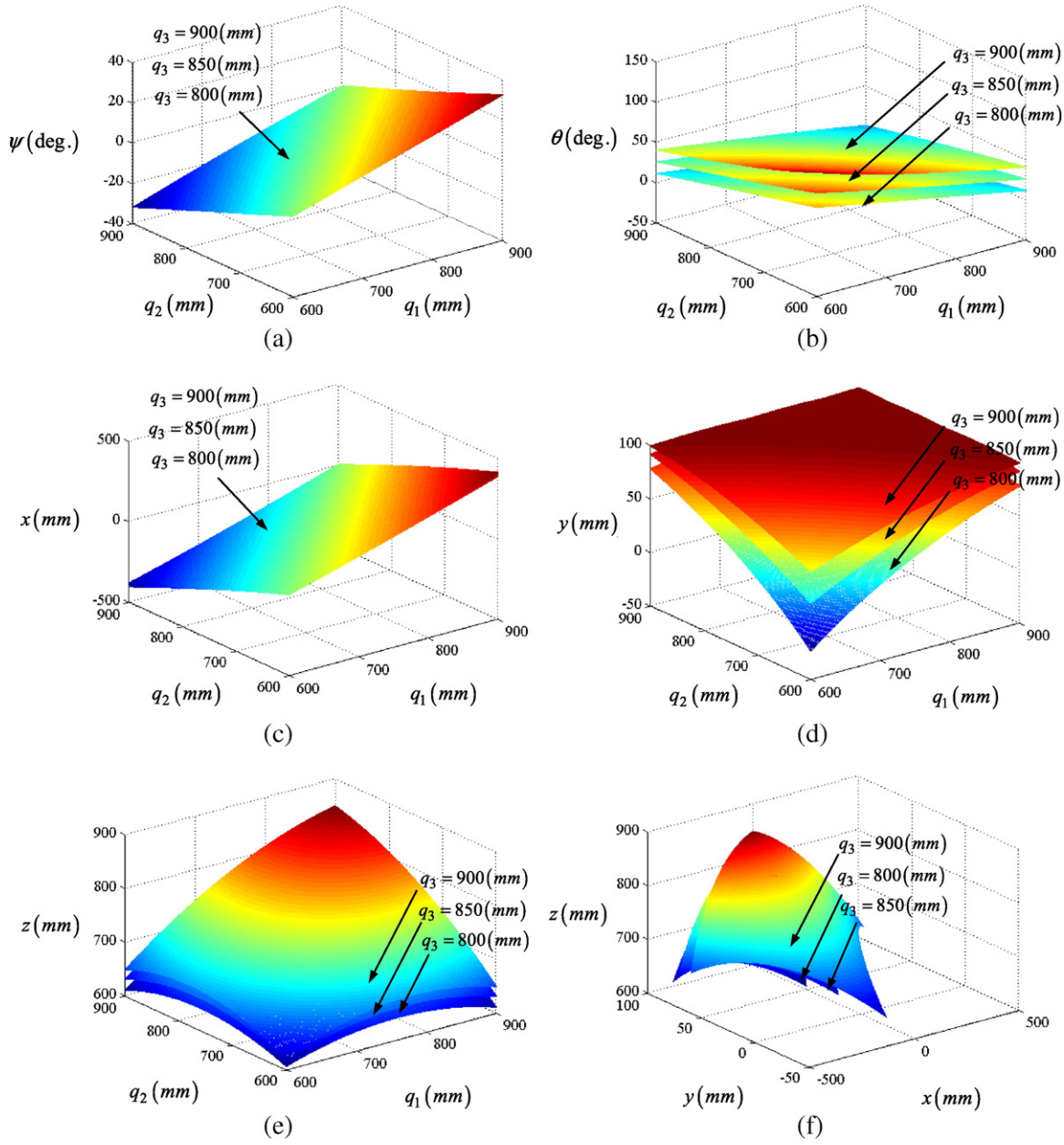

Fig. 7. The reachable workspace of the mechanism.

The approach followed in this paper for having an insight into the reachable workspace of the manipulator, considers the parasitic motion workspace. Fig. 7 (*a*) and Fig. 7 (*c*) show that, the distributions of ψ and *x* only have relation with the q_1 and q_2, regardless of the variation of q_3. The other parameters, including θ, *y* and z, are symmetrically distributed in the three-dimensional space.

7. Transmission performance analysis

Performance evaluation is one of most important issues in the analysis and design of parallel manipulators. A number of performance indices, such as workspace, dexterity indices, condition number, transmission angle, motion/force transmission indices, et al., have been proposed and applied to the performance evaluation of parallel manipulators [19,21–25]. As we know, the traditional transmission/pressure angle, which was originally introduced for evaluating the force transmission quality of single-loop linkages, is generally no longer applicable to evaluate the motion/force transmissibility of spatial parallel mechanisms, but for the parallel mechanism proposed in this paper, the two identical RPU limbs are in the same plane and axes of the two revolute joints are parallel to each other, and the axis of revolute joint of the SPR limb is parallel to *u* axis. Due to these joints arrangement mentioned above, the moving platform of the presented 3-DOF SPM exhibits a motion such that one of its point traces a planar curve (2DOF) and orientation of the platform is controlled about an axis tangent to that curve (1DOF). Thus, the pressure angle is applicable to evaluate the motion/force transmissibility of the proposed parallel mechanisms due to the structure characteristics.

In this section, performance analysis of the mechanism will be carried out based on the pressure angles between limbs. The definitions of the pressure angles between limbs are shown in Fig. 8.

For the RPU limb, angle α_i, as shown in Fig. 8(*a*), is the acute angle between the velocity (along $\boldsymbol{Qw}_2$ ($-\boldsymbol{Qw}_1$)) of point A_1 and the force (along $\boldsymbol{w}_1$, ($\boldsymbol{w}_2$)) imposed by the two RPU limbs at the same point. It represents the force/motion transmission capability from limb 2 (1) to limb 1 (2) under the condition that the actuated joint in limb 1 (2) is locked. α is the angle between the $\boldsymbol{w}_1$ and $\boldsymbol{w}_2$.

For the SPR limb, angle β_i, as shown in Fig. 8(*b*), is the acute angle between the velocity (along $\boldsymbol{Nw}_3$ ($-\boldsymbol{Nw}_4$)) of point A_3 and the force (along $\boldsymbol{w}_3$, ($\boldsymbol{w}_4$)) imposed by the link in limb SPR (BA_3) at the same point. It represents the force/motion transmission capability from limb SPR (BA_3) to limb BA_3 (SPR) under the condition that the actuated joint in limb BA_3 (SPR) is locked. β is the angle between the $\boldsymbol{w}_3$ and $\boldsymbol{w}_4$.

In order to evaluate the performance of the mechanism, the performance index of κ_1 and κ_2 are defined as

$$\begin{aligned} \kappa_1 &= \cos(\alpha) \\ \kappa_2 &= \cos(\beta) \end{aligned} \tag{42}$$

Using Eq. (42), we can obtain the local transmission performance of the mechanism as shown in Fig. 9.

8. Conclusions

The paper presented a 3-DOF SPM 2-RPU&SPR wherein the moving platform exhibits a motion such that one of its point tracks a planar curve (2DOF) and orientation of the platform is controlled about an axis tangent to that curve (1DOF). The concept has the computational advantage of unique forward and inverse kinematic analysis. Firstly, the mobility of the mechanism is analyzed based on screw theory, each RPU limb exerts one constraint force and one couple on the platform, SPR limb only exerts one constraint force on the platform. Both the inverse and the forward position analyses are analyzed, and the analytical solutions are obtained for these two problems, unlike most parallel robots, the proposed SPM has only one unique real answer to the inverse and forward kinematics. Therefore, both the path planning and the control problems of the mechanism are very simple. Additionally, the overall Jacobian matrix and the constrained Jacobian matrix of the mechanism are obtained. Furthermore, the parasitic motion workspace and the reachable workspace are obtained based on the forward position analysis. Finally, pressure angles

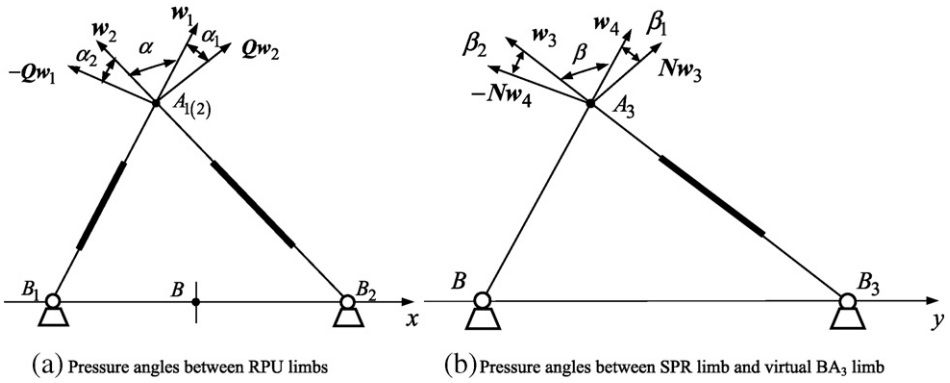

Fig. 8. Pressure angles between limbs.

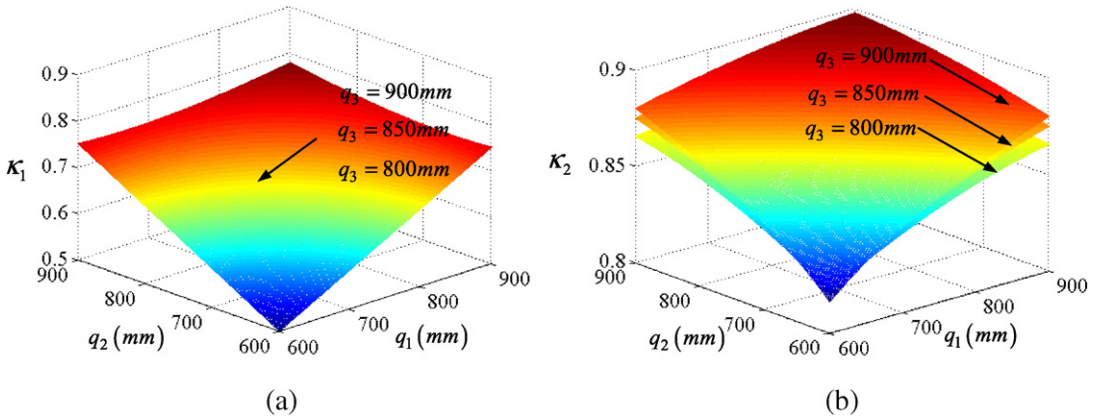

Fig. 9. Pressure angles between limbs.

have been used to evaluate the motion/force transmission performance of the manipulator. Based on the kinematics analysis of the mechanism, the inverse/forward dynamics analyses, the stiffness performance analysis and the kinematic optimization of the mechanism will be investigated in the future work.

Acknowledgments

The authors would like to express the sincere thanks to the referees for their valuable suggestions. This work was supported by the National Natural Science Foundation of China (NSFC) (Grant No. 51575544, 51205289 and 51275353). Macao Science and Technology Development Fund (110/2013/A3), Research Committee of University of Macau (MYRG2015-00194-FST, MYRG203(Y1-L4)-FST11-LYM). The authors also would like to thank the reviewers for their pertinent and helpful comments.

References

[1] K.H. Hunt, Structural kinematics of in-parallel-actuated robot arms, ASME J. Mech. Transm. Autom. Des. 105 (4) (1983) 705–712.
[2] R. Clavel, Delta - a fast robot with parallel geometry, Proc. 18th Int. Symp. Ind. Rob. 1988, pp. 91–100 (Lausanne, France).
[3] X. Liu, J. Kim, A new spatial three-DoF parallel manipulator with high rotational capability, IEEE/ASME Trans. Mechatron. 10 (5) (2005) 502–512.
[4] D. Zhang, Z. Bi, B. Li, Design and kinetostatic analysis of a new parallel manipulator, Robot. Comput. Integr. Manuf. 25 (2009) 782–791.
[5] F. Xie, X. Liu, J. Wang, A 3-DOF parallel manufacturing module and its kinematic optimization, Robot. Comput. Integr. Manuf. 28 (3) (2012) 334–343.
[6] E. Rodriguez-Leal, J.S. Dai, Evolutionary Design of Parallel Mechanisms: Kinematics of a Family of Parallel Mechanisms with Centralized Motion, Lambert Academic Publishing, 2010.
[7] E. Rodriguez-Leal, J.S. Dai, G.R. Pennock, A study of the mobility of 3-DOF parallel manipulators via screw theory, ASME Proc. Int. Des. Eng. Techn. Conf., Aug. 30–Sept. 2, 2009 (San Diego, CA).
[8] E. Cuan-Urquizo, E. Rodriguez-Leal, Kinematic analysis of the 3-CUP parallel mechanism, Robot. Comput. Integr. Manuf. 29 (5) (2013) 382–395.
[9] D. Zhang, X. Su, Z. Gao, J. Qian, Design, analysis and fabrication of a novel three degrees of freedom parallel robotic manipulator with decoupled motions, Int. J. Mech. Mater. Des. 9 (3) (2013) 199–212.
[10] J.A. Carretero, R.P. Podhorodeski, M.A. Nahon, Kinematic analysis and optimization of a new three degree-of-freedom spatial parallel manipulator, ASME Trans. J. Mech. Des. 122 (1) (2000) 17–24.
[11] G.E.E. Gojtan, G.P. Furtado, T.A. Hess-Coelho, Error analysis of a 3-DOF parallel mechanism for milling applications, ASME Trans. J. Mech. Rob. 5 (3) (2013) 034501.
[12] Y. Lou, J. Li, J. Shi, Z.X. Li, Development of a novel 3-DOF purely translational parallel mechanism, Proc. IEEE Int. Conf. Rob. Autom. 2007, pp. 169–174 (Roma, Italy).
[13] F. Gao, W.M. Li, X.C. Zhao, Z.L. Jin, H. Zhao, New kinematic structures for 2-, 3-, 4-, and 5-dof parallel manipulator design, Mech. Mach. Theory 37 (11) (2012) 1395–1411.
[14] Y.M. Li, Q. Xu, Kinematic analysis of a 3-PRS parallel manipulator, Robot. Comput. Integr. Manuf. 23 (4) (2007) 395–408.
[15] R. Di Gregorio, The 3-RRS wrist: a new, simple and non-overconstrained spherical parallel manipulator, ASME Trans. J. Mech. Des. 126 (5) (2004) 850–855.
[16] J. Dai, Z. Huang, H. Lipkin, Mobility of overconstrained parallel mechanisms, ASME J. Mech. Des. 128 (1) (2006) 220–229.
[17] J.J. Yu, X. Dong, X. Pei, X. Kong, Mobility and singularity analysis of a class of two degrees of freedom rotational parallel mechanisms using a visual graphic approach, ASME Trans. J. Mech. Rob. 4 (4) (2012) 041006.
[18] Y. Yun, Y.M. Li, A general dynamics and control model of a class of multi-DOF manipulators for active vibration control, Mech. Mach. Theory 46 (11) (2011) 1549–1574.
[19] T. Huang, S. Liu, J. Mei, D.G. Chetwynd, Optimal design of a 2-DOF pick-and-place parallel robot using dynamic performance indices and angular constraints, Mech. Mach. Theory 70 (2013) 246–253.
[20] W. Xu, Y.M. Li, Kinematics and workspace analysis for a novel 6-PSS parallel manipulator, IEEE Int. Conf. Rob. Biomim. 2013, pp. 1869–1874 (Shenzhen, China).
[21] J. Wang, C. Wu, X. Liu, Performance evaluation of parallel manipulators: motion/force transmissibility and its index, Mech. Mach. Theory 45 (10) (2010) 1462–1476.
[22] C. Wu, X. Liu, L. Wang, J. Wang, Optimal design of spherical 5R parallel manipulators considering the motion/force transmissibility, ASME J. Mech. Des. 132 (3) (2010) 0310021–03100210.
[23] C. Chen, J. Angeles, Generalized transmission index and transmission quality for spatial linkages, Mech. Mach. Theory 42 (9) (2007) 1225–1237.
[24] C. Lin, W. Chang, The force transmissibility index of planar linkage mechanisms, Mech. Mach. Theory 37 (12) (2002) 1465–1485.
[25] H. Liu, T. Huang, A. Kecskeméthy, D. Chetwynd, A generalized approach for computing the transmission index of parallel mechanisms, Mech. Mach. Theory 74 (2014) 245–256.